

Article

A Homotopy Method for the Constrained Inverse Problem in the Multiphase Porous Media Flow

Tao Liu ^{1,*} , Kaiwen Xia ¹, Yuanjin Zheng ², Yanxiong Yang ³, Ruofeng Qiu ³, Yunfei Qi ³ and Chao Liu ¹

¹ School of Mathematics and Statistics, Northeastern University at Qinhuangdao, Qinhuangdao 066004, China; xiakaiwenioy@163.com (K.X.); liuchao@mail.neu.edu.cn (C.L.)

² School of Electrical and Electronic Engineering, Nanyang Technological University, Singapore 639798, Singapore; yjzheng@ntu.edu.sg

³ Eighth Geological Brigade, Hebei Bureau of Geology and Mineral Resources Exploration, Qinhuangdao 066000, China; 13903355167@163.com (Y.Y.); qrofen1980@163.com (R.Q.); geo_yfqi@163.com (Y.Q.)

* Correspondence: liutao@neuq.edu.cn or math.taoliu@gmail.com

Abstract: This paper considers the constrained inverse problem based on the nonlinear convection-diffusion equation in the multiphase porous media flow. To solve this problem, a widely convergent homotopy method is introduced and proposed. To evaluate the performance of the mentioned method, two numerical examples are presented. This method turns out to have wide convergence region and strong anti-noise ability.

Keywords: inverse problem; homotopy method; multiphase porous media flow; constraints



Citation: Liu, T.; Xia, K.; Zheng, Y.; Yang, Y.; Qiu, R.; Qi, Y.; Liu, C. A Homotopy Method for the Constrained Inverse Problem in the Multiphase Porous Media Flow. *Processes* **2022**, *10*, 1143. <https://doi.org/10.3390/pr10061143>

Academic Editor: Md. Shakhaoath Khan

Received: 10 May 2022

Accepted: 6 June 2022

Published: 7 June 2022

Publisher's Note: MDPI stays neutral with regard to jurisdictional claims in published maps and institutional affiliations.



Copyright: © 2022 by the authors. Licensee MDPI, Basel, Switzerland. This article is an open access article distributed under the terms and conditions of the Creative Commons Attribution (CC BY) license (<https://creativecommons.org/licenses/by/4.0/>).

1. Introduction

The multiphase flow in porous media is of great importance in biology [1], chemistry [2], civil engineering [3], mechanics [4], and geosciences [5]. The porous media flow in many engineering problems, including reservoir engineering and reservoir simulation engineering, is often used to simulate the gas and oil flow within the reservoir. The authors in [6] proposed the fractional flow formulation of the multiphase flow equations in porous media, which leads to a nonlinear convection-diffusion saturation equation. Recently, Saeed et al. exactly analyzed the second grade fluid [7] and viscoelastic liquid with single slip assumption [8], and studied the natural convection flow [9] from in mathematical perspective. Abdeljawad et al. [10] and Firdous et al. [11], respectively, considered the MHD Maxwell fluid and Powell-Eyring fluid. Riaz et al. [12,13] mainly researched on the MHD Oldroyd-B fluid. Nowadays there are many different studies that aim to solve the inverse problem in multiphase porous media flow. Hazra et al. [14] solved the direct and inverse modeling in multiphase porous media flow using numerical simulation techniques, and Wang and Zabarar [15] identified the contamination source in multiphase porous media flow. Nilssen et al. [16] recovered the diffusion parameters in multiphase porous media flow with the augmented Lagrangian method. With the development of artificial intelligence, several recent studies focused on the application of deep learning models to the inverse problem in multiphase porous media flow [17–20].

This paper considers the identification of space-dependent permeability \mathbf{k} for the nonlinear convection-diffusion equation in the multiphase porous media flow:

$$u_t + \nabla \cdot (\phi, \varphi) - \nabla \cdot (\mathbf{k} \cdot N(u) \nabla u) = f(\mathbf{x}, t), \quad (\mathbf{x}, t) \in \Omega \times (0, T), \quad (1)$$

under the boundary and initial conditions

$$u(\mathbf{x}, t) = \chi(\mathbf{x}, t), \quad (\mathbf{x}, t) \in \partial\Omega \times (0, T), \quad (2)$$

$$u(\mathbf{x}, 0) = \psi(\mathbf{x}), \quad \mathbf{x} \in \Omega. \quad (3)$$

An additional condition is

$$u(\mathbf{x}^s, t) = \gamma(\mathbf{x}^s, t), \quad s = 1, 2, \dots, S, \quad t \in (0, T), \quad (4)$$

where ϕ and φ are both S-shaped Buckley–Leverett flux functions, N is a nonlinear diffusion function, f is a source function that is piecewise smooth, Ω is set to be an unit square for simplicity, and γ is the measured data (seepage velocity data).

Equation (1) correlates with the multiphase porous media flow. The partial differential equation (PDE) system describing the immiscible displacement of oil by water in porous media under no gravity condition is as follows [6]:

$$\begin{cases} \nabla \cdot \mathbf{V} = f_1(\mathbf{x}, t), \\ \mathbf{V} = -\mathbf{k} \cdot \zeta(\mathbf{x}, u)(\nabla p - \vartheta(u)\nabla h), \\ \beta(\mathbf{x})u_t + \nabla \cdot (\phi(u)\mathbf{V} + \mathbf{k} \cdot \varphi(u)\nabla h) - \nabla \cdot (\mathbf{k} \cdot N(u)\nabla u) = f_2(\mathbf{x}, t), \end{cases} \quad (5)$$

where $\phi = \frac{\zeta_{ra}}{\zeta}$, $\zeta_{ra} = \frac{\mathbf{k}_{ra}}{\mu}$, $\varphi = (\vartheta - \rho)\phi\epsilon$, and the definitions of model parameters are listed in Table 1. Units for \mathbf{k} , \mathbf{V} , p , h , ρ are, respectively, m^2 , m/s , N , m , kg/m^3 , and other parameters are dimensionless.

Table 1. Parameter definitions.

Parameter	Definition
\mathbf{k}	absolute permeability
\mathbf{V}	total Darcy velocity
ζ	total mobility of phases
p	global pressure
ϑ	density of wetting phase
h	height
β	porosity
f_1	injection well
f_2	production well
ζ_{ra}	mobility ratio
\mathbf{k}_{ra}	relative permeability
μ	viscosity
ρ	density
ϵ	phase mobility of nonwetting phase

Equation (1) closely resembles Equation (5) if the time derivative and convection terms are not considered. The coefficients of time derivative terms in Equations (1) and (5) are respectively constant 1 and $\beta(\mathbf{x})$; the convection term in Equation (5) has varying coefficient and permeability dependence, and the one in Equation (1) does not.

Oil reservoir simulation on the basis of this inverse problem is an effective tool, which can provide help for petroleum reservoir management, such as the choices of the fluid production and injection rates, well locations, imaging method (see Figure 1). Generally, the permeability model has problems with equivalence, non-uniqueness, hidden or suppressed layers and lack of model resolution, because the measured data are insufficient, inconsistent and inaccurate [21]. Moreover, the primary difficulties of the traditional methods (e.g., Levenberg–Marquardt, Gauss–Newton) are the local convergence property and that the cost function has numerous local minima. To cope with these problems, a homotopy method is developed associated with the constraints of well logs to identify the permeability coefficient.

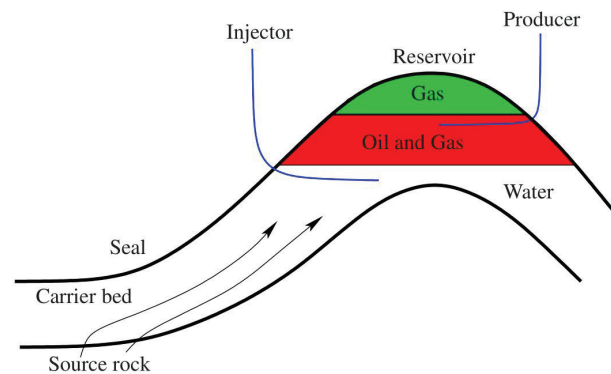


Figure 1. Practical description of the problem.

The homotopy method has global convergence under certain weak assumptions [22], and so has been successfully used to solve various nonlinear problems [23–28]. Recently, some authors also used it to solve inverse problems. For instance, Mallick et al. [29,30] used this method to estimate the thermal parameters within annular fins. Biswal et al. [31] applied the homotopy method for the inverse analysis of Jeffery–Hamel flow problem. Sattari Shajari and Shidfar [32] studied the homotopy solution of the wave equation inverse source problem. Liu [33,34] combined the homotopy method with multiscale ideas to develop the hybrid algorithm, and applied it to nonlinear inverse problems. Hu et al. [35] identified the parameters of a cracked beam using the homotopy algorithm. Courbot and Colicchio [36] analyzed the solution of the gridless sparse recovery problem using the homotopy method. The homotopy method has also been applied to the fractional inverse Stefan problem [37], the backward heat conduction problem [38], the porosity reconstruction on the basis of Biot elastic model [39], etc.

Usually, the measured data have a low signal-to-noise ratio. With the aim of restraining noise and improving identified model quality, the constraint condition has a wide application in many inversion fields [40–43]. The reason lies in that the constraint data are recorded from the interior of the model to be identified, and are less noisy than the measured data.

In previous works [44,45], we have verified the effectiveness of the homotopy and multigrid-homotopy methods for the inverse problem of the nonlinear diffusion equation:

$$u_t - \nabla \cdot (\mathbf{k} \cdot N(u, \nabla u) \nabla u) = f(\mathbf{x}, t), \quad (6)$$

which is an intermediate step of permeability identification in multiphase porous media flow. Different from [44,45], this paper not only considers the permeability identification based on the nonlinear convection-diffusion Equation (1), which can more accurately describe the multiphase flow process in porous media than the nonlinear diffusion Equation (6), but also introduces a well-log constraint to this inverse problem. The resulted constrained inverse problem can be transformed into a nonlinear constrained optimization problem. Because of the ill-posedness of problem and the local convergence property of traditional methods, we first impose Tikhonov regularization, and then use a widely convergent homotopy method to solve the normal equation of the regularized cost function. The final part of the paper consists of a report of numerical experiments that demonstrates the performance of the method.

2. Discretization

Equations (1)–(4) can be discretized by using the finite-difference scheme as follows:

$$\left\{ \begin{array}{l} \frac{u_{i,j}^k - u_{i,j}^{k-1}}{h_t} + \nabla \cdot (\phi(u_{i,j}^{k-1}), \varphi(u_{i,j}^{k-1})) - \nabla \cdot (\mathbf{k}_{i,j} N_{i,j}^k \nabla u_{i,j}^k) = f_{i,j}^k, \\ i = 1, \dots, I-1; \quad j = 1, \dots, J-1; \quad k = 1, \dots, K, \\ u_{0,j}^k = \chi_{0,j}^k, \quad j = 0, \dots, J; \quad k = 1, \dots, K, \\ u_{1,j}^k = \chi_{1,j}^k, \quad j = 0, \dots, J; \quad k = 1, \dots, K, \\ u_{i,0}^k = \chi_{i,0}^k, \quad i = 0, \dots, I; \quad k = 1, \dots, K, \\ u_{i,1}^k = \chi_{i,1}^k, \quad i = 0, \dots, I; \quad k = 1, \dots, K, \\ u_{i,j}^0 = \psi_{i,j}, \quad i = 0, \dots, I; \quad j = 0, \dots, J, \\ u_{x^s}^k = \gamma_{x^s}^k, \quad s = 1, \dots, S; \quad k = 1, \dots, K, \end{array} \right. \tag{7}$$

where

$$\begin{aligned} u_{i,j}^k &= u(ih_x, jh_y, kh_t), \quad \mathbf{k}_{i,j} = \mathbf{k}(ih_x, jh_y), \quad f_{i,j}^k = f(ih_x, jh_y, kh_t), \\ \psi_{i,j} &= \psi(ih_x, jh_y), \quad \chi_{i,j}^k = \chi(ih_x, jh_y, kh_t), \quad \gamma_{x^s}^k = \gamma(x^s, kh_t), \\ I &= 1/h_x, \quad J = 1/h_y, \quad K = T/h_t, \end{aligned}$$

h_t, h_x, h_y are, respectively, the time and spatial step lengths. $\nabla \cdot (\phi(u_{i,j}^{k-1}), \varphi(u_{i,j}^{k-1}))$ and $\nabla \cdot (\mathbf{k}_{i,j} N_{i,j}^k \nabla u_{i,j}^k)$ are, respectively, the discretizations of convection and diffusion terms, which will be described in the Appendices A and B.

By Equation (7), this inverse problem can be formulated as the following nonlinear operator equation:

$$R(\mathbf{K}) = \Gamma, \tag{8}$$

where

$$\begin{aligned} \mathbf{K}^\top &= (\mathbf{k}_{1,1}, \mathbf{k}_{1,2}, \dots, \mathbf{k}_{1,J}, \mathbf{k}_{2,1}, \mathbf{k}_{2,2}, \dots, \mathbf{k}_{2,J}, \dots, \mathbf{k}_{I,1}, \mathbf{k}_{I,2}, \dots, \mathbf{k}_{I,J}), \\ \Gamma^\top &= (\gamma_{x^1}^1, \gamma_{x^2}^1, \dots, \gamma_{x^S}^1, \gamma_{x^1}^2, \gamma_{x^2}^2, \dots, \gamma_{x^S}^2, \dots, \gamma_{x^1}^K, \gamma_{x^2}^K, \dots, \gamma_{x^S}^K). \end{aligned}$$

The measured data are denoted by $\tilde{\gamma}_{x^s}^k$, which can form the vector $\tilde{\Gamma}$ in the same sequence as Γ :

$$\tilde{\Gamma}^\top = (\tilde{\gamma}_{x^1}^1, \tilde{\gamma}_{x^2}^1, \dots, \tilde{\gamma}_{x^S}^1, \tilde{\gamma}_{x^1}^2, \tilde{\gamma}_{x^2}^2, \dots, \tilde{\gamma}_{x^S}^2, \dots, \tilde{\gamma}_{x^1}^K, \tilde{\gamma}_{x^2}^K, \dots, \tilde{\gamma}_{x^S}^K),$$

and the permeability, known from the well logs of a well located at point i_0 in the x -direction, is denoted by

$$\tilde{\mathbf{K}}_{i_0}^\top = (\tilde{\mathbf{k}}_{i_0,1}, \tilde{\mathbf{k}}_{i_0,2}, \dots, \tilde{\mathbf{k}}_{i_0,J}).$$

Let Y denote a matrix

$$Y = \begin{pmatrix} 0 & 0 & \dots & 0 & 1 & 0 & \dots & 0 & 0 & 0 & \dots & 0 \\ 0 & 0 & \dots & 0 & 0 & 1 & \dots & 0 & 0 & 0 & \dots & 0 \\ \vdots & \vdots & & \vdots & \vdots & \vdots & \ddots & \vdots & \vdots & \vdots & & \vdots \\ 0 & 0 & \dots & 0 & 0 & 0 & \dots & 1 & 0 & 0 & \dots & 0 \end{pmatrix}_{J \times (I \times J)},$$

such that $Y\mathbf{K} = (\mathbf{k}_{i_0,1}, \mathbf{k}_{i_0,2}, \dots, \mathbf{k}_{i_0,J})$, then Equation (8) turns into a nonlinear constrained optimization problem

$$\min_{\mathbf{K}} \|R(\mathbf{K}) - \tilde{\Gamma}\|^2, \quad \text{subject to } Y\mathbf{K} = \tilde{\mathbf{K}}_{i_0}. \tag{9}$$

By combining the objective function and constraint into a penalty function, we can attack Equation (9) by solving an unconstrained problem. For instance, a penalty function can be defined as

$$\|R(\mathbf{K}) - \tilde{\Gamma}\|^2 + \omega \|Y\mathbf{K} - \tilde{\mathbf{K}}_{i_0}\|^2, \tag{10}$$

where ω is the penalty parameter. After that, the solution of Equation (9) can be obtained by minimizing this unconstrained function Equation (10) for a large value of ω .

3. Identification Method

In the first part of this section, a basic iterative method is given by the successive linearization technique. Then, in the second part, the strategy used for the development of a homotopy method is presented.

3.1. Basic Iterative Method

It is common knowledge that the inverse problem is ill-posed, therefore the regularization technique has to be used for the improvement of numerical stability of the algorithm:

$$\min_{\mathbf{K}} \{ \|R(\mathbf{K}) - \bar{\Gamma}\|^2 + \omega \|Y\mathbf{K} - \bar{\mathbf{K}}_{i_0}\|^2 + \omega_1 \|W_1\mathbf{K}\|^2 + \omega_2 \|W_2\mathbf{K}\|^2 \}, \quad (11)$$

where ω_1, ω_2 denote the regularization parameters, W_1, W_2 denote, respectively, the second-order smooth matrices in the x - and y -direction.

$$W_1\mathbf{K} = \begin{bmatrix} 0 \\ \mathbf{k}_{1,1} - 2\mathbf{k}_{2,1} + \mathbf{k}_{3,1} \\ \mathbf{k}_{2,1} - 2\mathbf{k}_{3,1} + \mathbf{k}_{4,1} \\ \dots \\ \mathbf{k}_{I-2,1} - 2\mathbf{k}_{I-1,1} + \mathbf{k}_{I,1} \\ 0 \\ 0 \\ \mathbf{k}_{1,2} - 2\mathbf{k}_{2,2} + \mathbf{k}_{3,2} \\ \mathbf{k}_{2,2} - 2\mathbf{k}_{3,2} + \mathbf{k}_{4,2} \\ \dots \\ \mathbf{k}_{I-2,2} - 2\mathbf{k}_{I-1,2} + \mathbf{k}_{I,2} \\ 0 \\ \dots \\ 0 \\ \mathbf{k}_{1,J} - 2\mathbf{k}_{2,J} + \mathbf{k}_{3,J} \\ \mathbf{k}_{2,J} - 2\mathbf{k}_{3,J} + \mathbf{k}_{4,J} \\ \dots \\ \mathbf{k}_{I-2,J} - 2\mathbf{k}_{I-1,J} + \mathbf{k}_{I,J} \\ 0 \end{bmatrix}, W_2\mathbf{K} = \begin{bmatrix} 0 \\ \mathbf{k}_{1,1} - 2\mathbf{k}_{1,2} + \mathbf{k}_{1,3} \\ \mathbf{k}_{1,2} - 2\mathbf{k}_{1,3} + \mathbf{k}_{1,4} \\ \dots \\ \mathbf{k}_{1,J-2} - 2\mathbf{k}_{1,J-1} + \mathbf{k}_{1,J} \\ 0 \\ 0 \\ \mathbf{k}_{2,1} - 2\mathbf{k}_{2,2} + \mathbf{k}_{2,3} \\ \mathbf{k}_{2,2} - 2\mathbf{k}_{2,3} + \mathbf{k}_{2,4} \\ \dots \\ \mathbf{k}_{2,J-2} - 2\mathbf{k}_{2,J-1} + \mathbf{k}_{2,J} \\ 0 \\ \dots \\ 0 \\ \mathbf{k}_{I,1} - 2\mathbf{k}_{I,2} + \mathbf{k}_{I,3} \\ \mathbf{k}_{I,2} - 2\mathbf{k}_{I,3} + \mathbf{k}_{I,4} \\ \dots \\ \mathbf{k}_{I,J-2} - 2\mathbf{k}_{I,J-1} + \mathbf{k}_{I,J} \\ 0 \end{bmatrix}.$$

It is easy to show that Equation (11) is equivalent to (its normal equation):

$$R'(\mathbf{K})^\top (R(\mathbf{K}) - \bar{\Gamma}) + \omega Y^\top (Y\mathbf{K} - \bar{\mathbf{K}}_{i_0}) + (\omega_1 W_1^\top W_1 + \omega_2 W_2^\top W_2)\mathbf{K} = 0. \quad (12)$$

For the sake of avoiding the influence of second derivative, a successive linearization method can be introduced to construct a basic iterative method.

We first assume that the k th approximation \mathbf{K}^k of Equation (12) has been obtained, and use the linear function

$$E_k(\mathbf{K}) = R'(\mathbf{K}^k)(\mathbf{K} - \mathbf{K}^k) + R(\mathbf{K}^k),$$

instead of $R(\mathbf{K})$ in Equation (12):

$$R'(\mathbf{K}^k)^\top (R'(\mathbf{K}^k)(\mathbf{K} - \mathbf{K}^k) + R(\mathbf{K}^k) - \bar{\Gamma}) + \omega Y^\top (Y\mathbf{K} - \bar{\mathbf{K}}_{i_0}) + (\omega_1 W_1^\top W_1 + \omega_2 W_2^\top W_2)\mathbf{K} = 0. \quad (13)$$

Then, by denoting the solution of Equation (13) as \mathbf{K}^{k+1} , we obtain the basic iterative scheme:

$$\begin{cases} \mathbf{K}^{k+1} = \mathbf{K}^k + \Delta\mathbf{K}^k, & k = 0, 1, 2, \dots \\ [R'(\mathbf{K}^k)^\top R'(\mathbf{K}^k) + \omega Y^\top Y + \varpi_1 W_1^\top W_1 + \varpi_2 W_2^\top W_2] \Delta\mathbf{K}^k = \\ -[R'(\mathbf{K}^k)^\top (R(\mathbf{K}^k) - \bar{\Gamma}) + \omega Y^\top (Y\mathbf{K}^k - \bar{\mathbf{K}}_{i_0}) \\ + (\varpi_1 W_1^\top W_1 + \varpi_2 W_2^\top W_2) \mathbf{K}^k]. \end{cases} \quad (14)$$

This method is fast and stable, but only has local convergence.

3.2. Homotopy Method

In order to expand the domain of convergence, the homotopy method is introduced to solve Equation (12) by taking into account the fixed-point homotopy equation

$$\begin{aligned} A(\mathbf{K}, a) = & a[R'(\mathbf{K})^\top (R(\mathbf{K}) - \bar{\Gamma}) + \omega Y^\top (Y\mathbf{K} - \bar{\mathbf{K}}_{i_0}) \\ & + (\varpi_1 W_1^\top W_1 + \varpi_2 W_2^\top W_2) \mathbf{K}] + (1 - a)(\mathbf{K} - \mathbf{K}_0) = 0, \end{aligned} \quad (15)$$

where $a \in [0, 1]$ and \mathbf{K}_0 are, respectively, the homotopy parameter and arbitrary initial value. From Equation (15), it is easy to see

$$\begin{aligned} A(\mathbf{K}, 0) &= \mathbf{K} - \mathbf{K}_0, \\ A(\mathbf{K}, 1) &= R'(\mathbf{K})^\top (R(\mathbf{K}) - \bar{\Gamma}) + \omega Y^\top (Y\mathbf{K} - \bar{\mathbf{K}}_{i_0}) \\ &+ (\varpi_1 W_1^\top W_1 + \varpi_2 W_2^\top W_2) \mathbf{K}. \end{aligned} \quad (16)$$

As the homotopy parameter a changed continuously from 0 to 1, the trivial problem $A(\mathbf{K}, 0) = 0$ is continuously deformed to the original problem $A(\mathbf{K}, 1) = 0$, that is, \mathbf{K} is changed from \mathbf{K}_0 to the solution of Equation (12). In topology, this is called deformation.

To achieve the specific numerical algorithm, we first divide the interval $[0, 1]$ into $0 = a_0 < a_1 < \dots < a_B = 1$, and then solve $A(\mathbf{K}, a_b) = 0$ ($b = 1, 2, \dots, B$) sequentially by some iterative scheme, whose initial value is chosen as the solution \mathbf{K}_{b-1} of the previous equation $A(\mathbf{K}, a_{b-1}) = 0$.

For $A(\mathbf{K}, a_b) = 0$, in the same manner as the construction of Equation (14), we have

$$\begin{cases} \mathbf{K}_b^{k+1} = \mathbf{K}_b^k + \Delta\mathbf{K}_b^k, & k = 0, 1, \dots, b_m, \\ [a_b R'(\mathbf{K}_b^k)^\top R'(\mathbf{K}_b^k) + a_b \omega Y^\top Y + a_b \varpi_1 W_1^\top W_1 + a_b \varpi_2 W_2^\top W_2 + (1 - a_b)I] \Delta\mathbf{K}_b^k = \\ -[a_b R'(\mathbf{K}_b^k)^\top (R(\mathbf{K}_b^k) - \bar{\Gamma}) + a_b \omega Y^\top (Y\mathbf{K}_b^k - \bar{\mathbf{K}}_{i_0}) \\ + (a_b \varpi_1 W_1^\top W_1 + a_b \varpi_2 W_2^\top W_2) \mathbf{K}_b^k + (1 - a_b)(\mathbf{K}_b^k - \mathbf{K}_0)], \\ \mathbf{K}_b^0 = \mathbf{K}_{b-1}, \quad \mathbf{K}_b = \mathbf{K}_b^{b_m+1}, \quad b = 1, 2, \dots, B, \end{cases} \quad (17)$$

where I refers to the unit matrix. After \mathbf{K}_B is obtained, Equation (14) may be used to make correction. Therefore, Equations (14) and (17) are combined into a stabilized method which has a wider domain of convergence for the constrained permeability identification of the nonlinear convection-diffusion equation.

By choosing $a_b = \frac{b}{B}$ and $b_m = 0$, Equation (17) can be simplified as

$$\begin{cases} \mathbf{K}_{b+1} = \mathbf{K}_b + \Delta\mathbf{K}_b, & b = 0, 1, \dots, B - 1, \\ [\frac{b}{B} R'(\mathbf{K}_b)^\top R'(\mathbf{K}_b) + \frac{b}{B} \omega Y^\top Y + \frac{b}{B} \varpi_1 W_1^\top W_1 + \frac{b}{B} \varpi_2 W_2^\top W_2 + (1 - \frac{b}{B})I] \Delta\mathbf{K}_b = \\ -[\frac{b}{B} R'(\mathbf{K}_b)^\top (R(\mathbf{K}_b) - \bar{\Gamma}) + \frac{b}{B} \omega Y^\top (Y\mathbf{K}_b - \bar{\mathbf{K}}_{i_0}) \\ + (\frac{b}{B} \varpi_1 W_1^\top W_1 + \frac{b}{B} \varpi_2 W_2^\top W_2) \mathbf{K}_b + (1 - \frac{b}{B})(\mathbf{K}_b - \mathbf{K}_0)]. \end{cases} \quad (18)$$

To test the necessity of introduction of constraints, we also give the homotopy method for the ordinary permeability identification for the nonlinear convection-diffusion equation in the multiphase porous media flow, and compare Equations (14) and (18) with it.

Specifically, let $\omega = 0$, then Equations (14) and (18) turn into the homotopy method for the ordinary permeability identification problem

$$\begin{cases} \mathbf{K}_{b+1} = \mathbf{K}_b + \Delta\mathbf{K}_b, & b = 0, 1, \dots, B - 1, \\ \left[\frac{b}{B} R'(\mathbf{K}_b)^\top R'(\mathbf{K}_b) + \frac{b}{B} \omega_1 W_1^\top W_1 + \frac{b}{B} \omega_2 W_2^\top W_2 + (1 - \frac{b}{B}) I \right] \Delta\mathbf{K}_b = \\ - \left[\frac{b}{B} R'(\mathbf{K}_b)^\top (R(\mathbf{K}_b) - \bar{\Gamma}) + (\frac{b}{B} \omega_1 W_1^\top W_1 + \frac{b}{B} \omega_2 W_2^\top W_2) \mathbf{K}_b \right. \\ \left. + (1 - \frac{b}{B})(\mathbf{K}_b - \mathbf{K}_0) \right], \end{cases} \quad (19)$$

and

$$\begin{cases} \mathbf{K}^{k+1} = \mathbf{K}^k + \Delta\mathbf{K}^k, & k = 0, 1, 2, \dots \\ \left[R'(\mathbf{K}^k)^\top R'(\mathbf{K}^k) + \omega_1 W_1^\top W_1 + \omega_2 W_2^\top W_2 \right] \Delta\mathbf{K}^k = \\ - \left[R'(\mathbf{K}^k)^\top (R(\mathbf{K}^k) - \bar{\Gamma}) + (\omega_1 W_1^\top W_1 + \omega_2 W_2^\top W_2) \mathbf{K}^k \right]. \end{cases} \quad (20)$$

4. Numerical Experiments

This section tested two synthetic examples to show the performance of our proposed method. The parameters required in the identification process are given by

$$\begin{aligned} \phi(u) &= \frac{u^2(1 - 5(1 - u^2))}{u^2 + (1 - u)^2}, & \varphi(u) &= \frac{u^2}{u^2 + (1 - u)^2}, & N(u) &= u^2 - u + 1, \\ \psi(\mathbf{x}) &= \sin(\pi x)\sin(\pi y), & \chi(\mathbf{x}, t) &= 0, & \omega &= 10^4, & \omega_1 = \omega_2 &= 10^{-5}, \\ \mathbf{K}_0 &\equiv 5, & h_x = h_y &= \frac{1}{24}, & i_0 &= \frac{12}{24}, & T &= 0.06, & h_t &= 0.002, & B &= 5. \end{aligned}$$

Example 1. The exact permeability \mathbf{k} in this example is shown in Figure 2. In order to illustrate the noise sensitivity, we add Gaussian noise to the measured data $\bar{\Gamma}$. With 5%, 10%, 15%, and 20% Gaussian noises, the identified permeability results by the homotopy method with constraints are shown in Figures 3–6, respectively.

Example 2. This example selects a model of two anomalous bodies in a homogeneous medium with a permeability of 4.25, and the anomalous bodies have the permeability of 6.18 and 7.55, see Figure 7. Figures 8–11, respectively, show the identified permeability results of the homotopy method with constraints, with 5%, 10%, 15%, and 20% Gaussian noises.

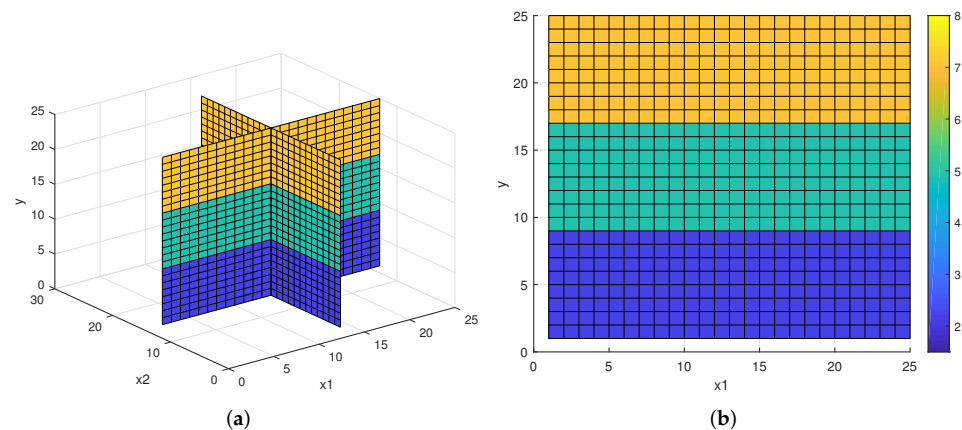


Figure 2. The exact permeability \mathbf{k} in Example 1. (a) Three-dimensional model. (b) Two-dimensional profile.

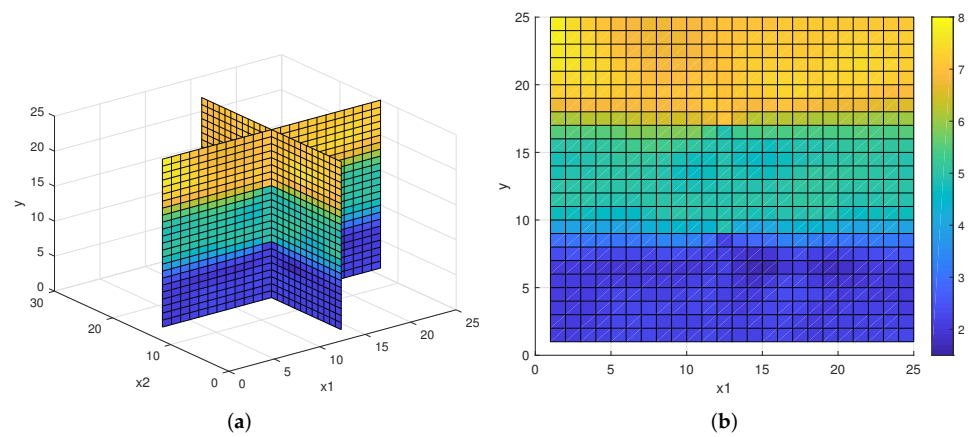


Figure 3. The identified permeability k with 5% Gaussian noise in Example 1. (a) Three-dimensional model. (b) Two-dimensional profile.

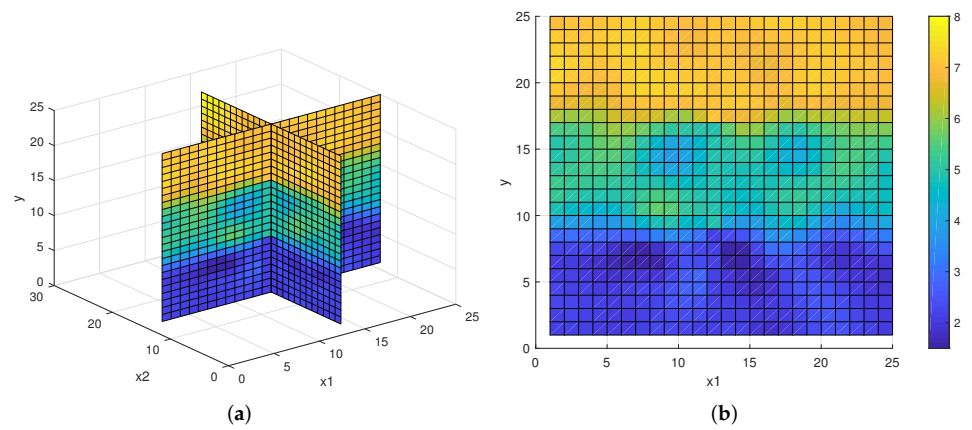


Figure 4. The identified permeability k with 10% Gaussian noise in Example 1. (a) Three-dimensional model. (b) Two-dimensional profile.

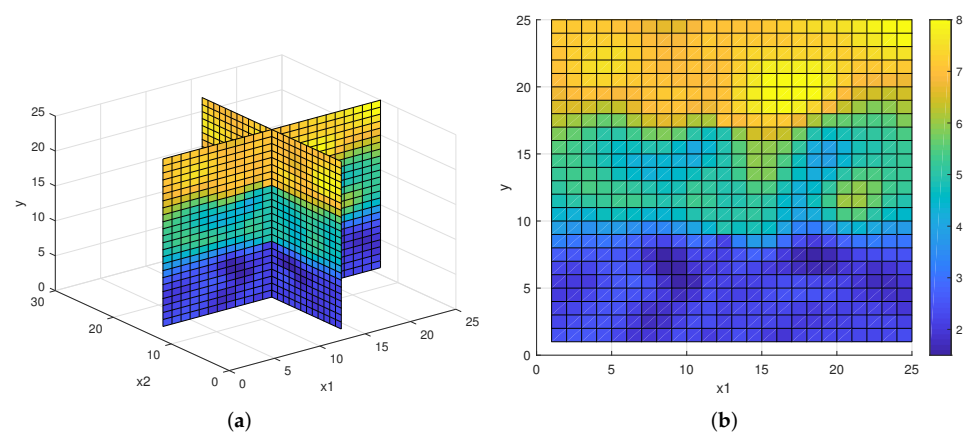


Figure 5. The identified permeability k with 15% Gaussian noise in Example 1. (a) Three-dimensional model. (b) Two-dimensional profile.

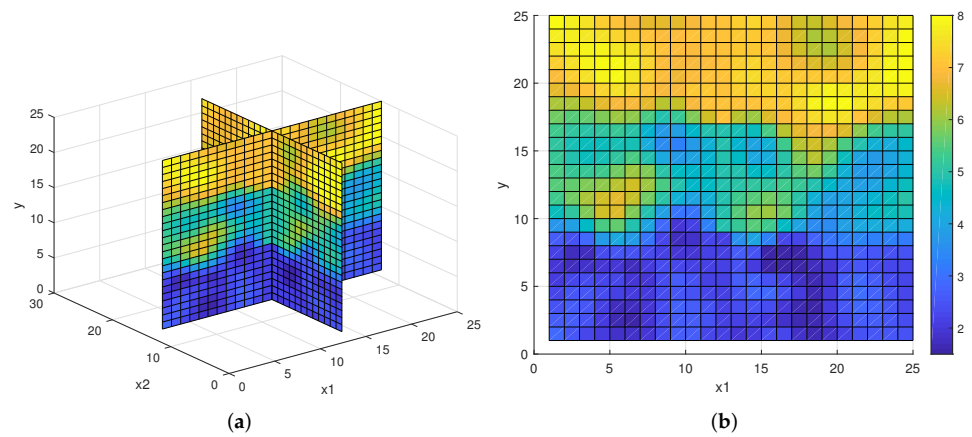


Figure 6. The identified permeability k with 20% Gaussian noise in Example 1. (a) Three-dimensional model. (b) Two-dimensional profile.

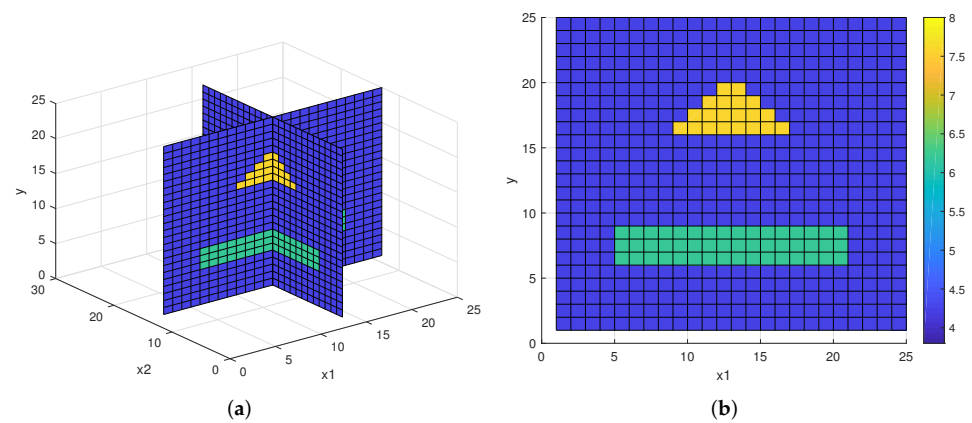


Figure 7. The exact permeability k in Example 2. (a) Three-dimensional model. (b) Two-dimensional profile.

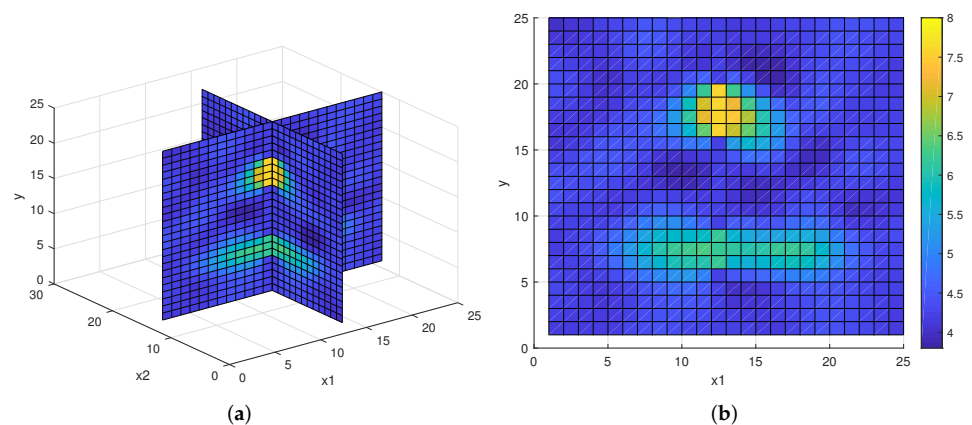


Figure 8. The identified permeability k with 5% Gaussian noise in Example 2. (a) Three-dimensional model. (b) Two-dimensional profile.

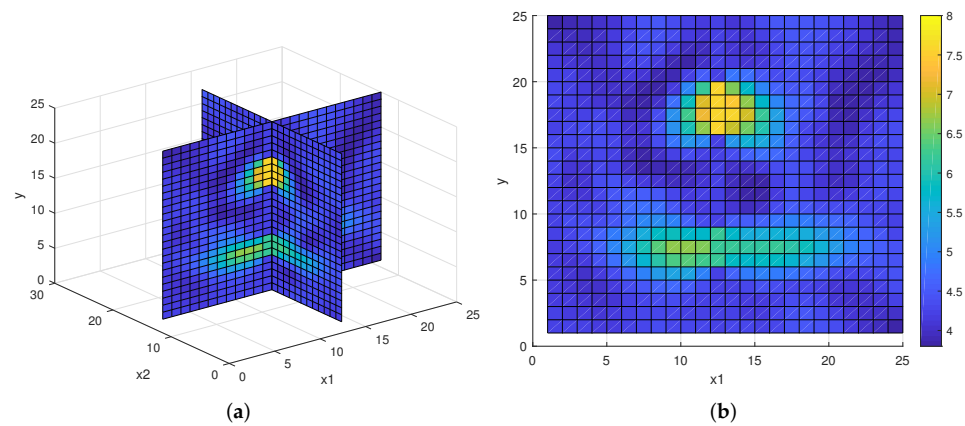


Figure 9. The identified permeability k with 10% Gaussian noise in Example 2. (a) Three-dimensional model. (b) Two-dimensional profile.

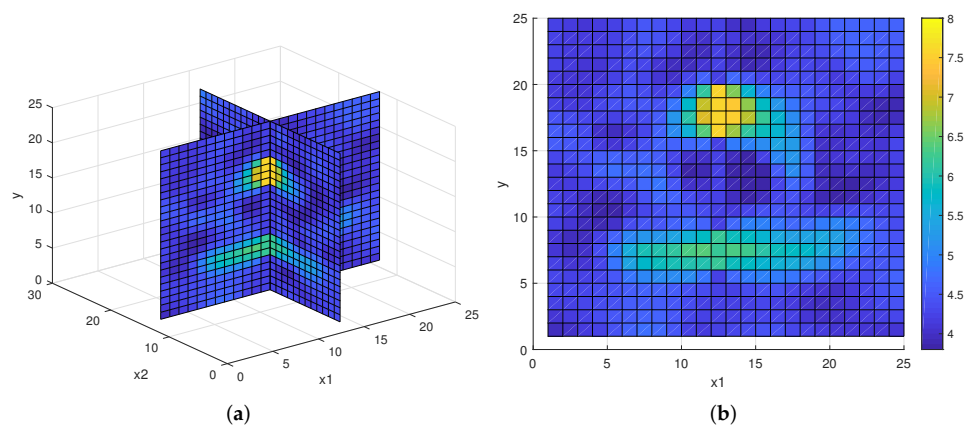


Figure 10. The identified permeability k with 15% Gaussian noise in Example 2. (a) Three-dimensional model. (b) Two-dimensional profile.

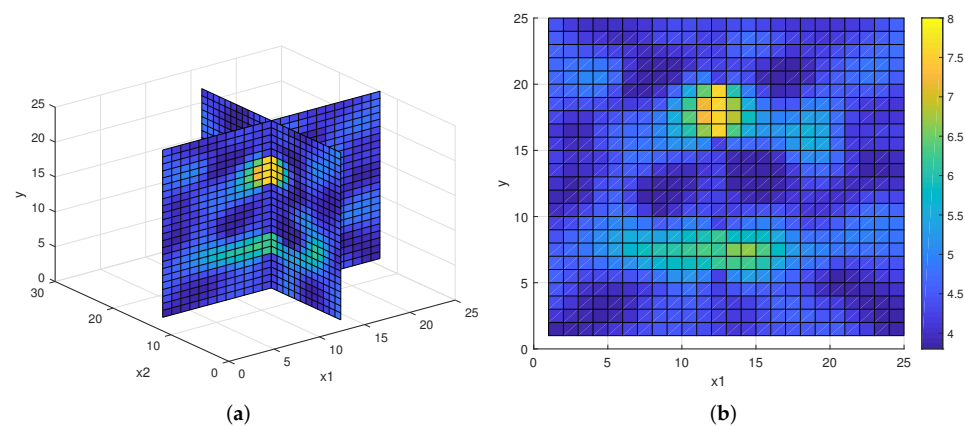


Figure 11. The identified permeability k with 20% Gaussian noise in Example 2. (a) Three-dimensional model. (b) Two-dimensional profile.

To test the necessity of introduction of constraints and the wide convergence of the homotopy strategy, the homotopy method without constraints and basic iterative method with constraints are used for the above measured data, and the relative errors of all the identified permeability results by the three methods are listed in Table 2, where \times means that there is no convergent result.

Table 2 shows that

- (1) The stability of the homotopy method with constraints is better than the homotopy method without constraints;
- (2) The region of convergence of the homotopy strategy is wider than the basic iterative method with constraints;
- (3) The homotopy method with constraints has wide convergence region and strong anti-noise ability.

Table 2. Relative errors of identified permeability \mathbf{k} by three different methods. HM—homotopy method with constraints, HM—homotopy method without constraints, BIMC—basic iterative method with constraints.

Example Number	Noise Level	HMC	HM	BIMC
4.1	5%	6.22%	6.90%	×
	10%	6.38%	7.40%	×
	15%	7.13%	×	×
	20%	7.44%	×	×
4.2	5%	5.71%	6.47%	×
	10%	5.81%	7.39%	×
	15%	6.06%	×	×
	20%	7.19%	×	×

5. Conclusions

To restrain the noise and improve identified model quality, the constraint condition is introduced to the inverse problem of the nonlinear convection-diffusion equation in the multiphase porous media flow. Then, Tikhonov regularization is applied to the constrained optimization problem obtained by the discretization to overcome the ill-posed property. We developed a homotopy method that is widely convergent. The results from the numerical experiments show that this method is feasible and effective. Compared with the homotopy method without constraints, our approach has better stability; compared with the basic iterative method with constraints, our approach has a wider convergence region. So far, there is no literature on the use of fractional operators for constraint inverse problems, which will be an interesting future work.

Author Contributions: Conceptualization, T.L. and Y.Z.; methodology, T.L. and Y.Z.; software, T.L. and K.X.; validation, T.L. and K.X.; formal analysis, T.L. and K.X.; investigation, T.L. and K.X.; resources, Y.Y., R.Q. and Y.Q.; data curation, T.L.; writing—original draft preparation, T.L., K.X. and Y.Z.; writing—review and editing, T.L., K.X. and Y.Z.; visualization, T.L.; supervision, Y.Z.; project administration, T.L., Y.Q. and C.L.; funding acquisition, T.L., Y.Q. and C.L. All authors have read and agreed to the published version of the manuscript.

Funding: This research was funded by the Natural Science Foundation of He-bei Province of China (A2020501005, A2020501007), the Fundamental Research Funds for the Central Universities (N2123015).

Institutional Review Board Statement: Not applicable.

Informed Consent Statement: Not applicable.

Data Availability Statement: Not applicable.

Acknowledgments: On behalf of my co-authors, we would like to express our great appreciation to the editor and reviewers.

Conflicts of Interest: The authors declare no conflict of interest.

Appendix A. Discretization of the Diffusion Term

Let

$$D_-^x u_{i,j}^k = \frac{u_{i,j}^k - u_{i-1,j}^k}{h_x}, \quad D_+^x u_{i,j}^k = \frac{u_{i+1,j}^k - u_{i,j}^k}{h_x},$$

be the discrete derivatives of x , and a corresponding notation is used for the the discrete derivatives of y .

The mean values for the discretized permeability are defined as

$$\bar{\mathbf{k}}_{i,j+\frac{1}{2}}^x = \frac{1}{2}(\mathbf{k}_{i+\frac{1}{2},j+\frac{1}{2}} + \mathbf{k}_{i-\frac{1}{2},j+\frac{1}{2}}), \quad \bar{\mathbf{k}}_{i+\frac{1}{2},j}^y = \frac{1}{2}(\mathbf{k}_{i+\frac{1}{2},j+\frac{1}{2}} + \mathbf{k}_{i+\frac{1}{2},j-\frac{1}{2}}),$$

and the mean values for the nonlinear diffusion function are defined as

$$(\bar{N}^x)_{i+\frac{1}{2},j}^k = \frac{1}{2}(N_{i+1,j}^k + N_{i,j}^k), \quad (\bar{N}^y)_{i,j+\frac{1}{2}}^k = \frac{1}{2}(N_{i,j+1}^k + N_{i,j}^k),$$

where $N_{i,j}^k = N(u_{i,j}^k)$.

Then, the diffusion term can be discretized as

$$\nabla \cdot (\mathbf{k}_{i,j} N_{i,j}^k \nabla u_{i,j}^k) = D_-^x (\bar{\mathbf{k}}_{i+\frac{1}{2},j}^y (\bar{N}^x)_{i+\frac{1}{2},j}^k D_+^x u_{i,j}^k) + D_-^y (\bar{\mathbf{k}}_{i,j+\frac{1}{2}}^x (\bar{N}^y)_{i,j+\frac{1}{2}}^k D_+^y u_{i,j}^k).$$

Appendix B. Discretization of the Convection Term

The convection term can be discretized by the Engquist–Osher upwind scheme [46] as follows:

$$\nabla \cdot (\phi(u_{i,j}^{k-1}), \phi(u_{i,j}^{k-1})) = D_-^x \phi^{EO}(u_{i,j}^{k-1}, u_{i+1,j}^{k-1}) + D_-^y \phi^{EO}(u_{i,j}^{k-1}, u_{i,j+1}^{k-1}),$$

where the Engquist–Osher numerical flux functions $\phi^{EO}(u_{i,j}^{k-1}, u_{i+1,j}^{k-1})$ and $\phi^{EO}(u_{i,j}^{k-1}, u_{i,j+1}^{k-1})$ are defined by

$$\begin{aligned} \phi^{EO}(u_{i,j}^{k-1}, u_{i+1,j}^{k-1}) &= \frac{1}{2}(\phi(u_{i,j}^{k-1}) + \phi(u_{i+1,j}^{k-1})) - \frac{1}{2} \int_{u_{i,j}^{k-1}}^{u_{i+1,j}^{k-1}} |\phi'(\xi)| d\xi, \\ \phi^{EO}(u_{i,j}^{k-1}, u_{i,j+1}^{k-1}) &= \frac{1}{2}(\phi(u_{i,j}^{k-1}) + \phi(u_{i,j+1}^{k-1})) - \frac{1}{2} \int_{u_{i,j}^{k-1}}^{u_{i,j+1}^{k-1}} |\phi'(\xi)| d\xi. \end{aligned}$$

Finally, we give the explicit formulas for ϕ^{EO} and φ^{EO} , for examples of $\phi(u) = \frac{u^2(1-5(1-u^2))}{u^2+(1-u)^2}$ and $\varphi(u) = \frac{u^2}{u^2+(1-u)^2}$. For the sake of simplicity, the following calculations only use one subscript index.

Appendix B.1. Buckley–Leverett Flux Function

$\varphi(u)$ is an S-shaped flux function of Buckley–Leverett type, and

$$\varphi'(u) \geq 0, \quad u \in (0, 1),$$

therefore

$$\varphi^{EO}(u_i, u_{i+1}) = \varphi(u_i).$$

Appendix B.2. Buckley–Leverett Flux Function with Gravitational Effects

$\phi(u)$ is an S-shaped flux function of Buckley–Leverett type under gravity effects, and for the calculation of $\int_{u_i}^{u_{i+1}} |\phi'(\xi)| d\xi$, we first discuss the sign of ϕ' in $(0, 1)$. Actually, ϕ' has only one zero point in $(0, 1)$, that is

$$x_{zero} \approx 0.37.$$

Therefore, we can get

$$\phi'(\xi) \begin{cases} < 0, & \xi \in (0, x_{zero}), \\ = 0, & \xi = x_{zero}, \\ > 0, & \xi \in (x_{zero}, 1). \end{cases}$$

Additionally, we have the formula of the integral

$$\int_{u_i}^{u_{i+1}} |\phi'(\xi)| d\xi = \begin{cases} \phi(u_{i+1}) - \phi(u_i), & u_i, u_{i+1} \geq x_{zero}, \\ \phi(u_i) - \phi(u_{i+1}), & u_i, u_{i+1} < x_{zero}, \\ \phi(u_i) + \phi(u_{i+1}) - 2\phi(x_{zero}), & u_i < x_{zero}, u_{i+1} \geq x_{zero}, \\ 2\phi(x_{zero}) - \phi(u_i) - \phi(u_{i+1}), & u_i \geq x_{zero}, u_{i+1} < x_{zero}, \end{cases}$$

and according to the definition of ϕ^{EO} , then we have

$$\phi^{EO}(u_i, u_{i+1}) = \begin{cases} \phi(u_i), & u_i, u_{i+1} \geq x_{zero}, \\ \phi(u_{i+1}), & u_i, u_{i+1} < x_{zero}, \\ \phi(x_{zero}), & u_i < x_{zero}, u_{i+1} \geq x_{zero}, \\ \phi(u_i) + \phi(u_{i+1}) - \phi(x_{zero}), & u_i \geq x_{zero}, u_{i+1} < x_{zero}. \end{cases}$$

References

- Rana, B.M.J.; Arifuzzaman, S.M.; Islam, S.; Reza-E-Rabbi, S.; Al-Mamun, A.; Mazumder, M.; Roy, K.C.; Khan, M.S. Swimming of microbes in blood flow of nano-bioconvective Williamson fluid. *Therm. Sci. Eng. Progr.* **2021**, *25*, 101018. [[CrossRef](#)]
- Reza-E-Rabbi, S.; Ahmmed, S.F.; Arifuzzaman, S.M.; Sarkar, T.; Khan, M.S. Computational modelling of multiphase fluid flow behaviour over a stretching sheet in the presence of nanoparticles. *Eng. Sci. Technol. Int. J.* **2020**, *23*, 605–617. [[CrossRef](#)]
- Moosavian, N. Pipe network modeling for analysis of flow in porous media. *Can. J. Civil Eng.* **2019**, *46*, 1151–1159. [[CrossRef](#)]
- Shapiro, A.A. Mechanics of the separating surface for a two-phase co-current flow in a porous medium. *Transp. Porous Med.* **2016**, *112*, 489–517. [[CrossRef](#)]
- Hunt, A.G.; Sahimi, M. Flow, transport, and reaction in porous media: Percolation scaling, critical-path analysis, and effective medium approximation. *Rev. Geoph.* **2017**, *55*, 993–1078. [[CrossRef](#)]
- Espedal, M.S.; Karlsen, K.H. Numerical solution of reservoir flow models based on large time step operator splitting algorithm. In *Filtration in Porous Media and Industrial Applications: Lecture Notes in Mathematics*; Fasano, A., Ed.; Springer: Berlin/Heidelberg, Germany, 2000; Volume 1734, pp. 9–77.
- Saeed, S.T.; Riaz, M.B.; Baleanu, D.; Akgul, A.; Husnine, S.M. Exact analysis of second grade fluid with generalized boundary conditions. *Intell. Autom. Soft Comput.* **2021**, *28*, 547–559. [[CrossRef](#)]
- Saeed, S.T.; Abro, K.A.; Almani, S. Role of single slip assumption on the viscoelastic liquid subject to non-integer differentiable operators. *Math. Meth. Appl. Sci.* **2021**, *44*, 6005–6020. [[CrossRef](#)]
- Saeed, S.T.; Riaz, M.B.; Baleanu, D.; Abro, K.A. A mathematical study of natural convection flow through a channel with non-singular kernels: An application to transport phenomena. *Alex. Eng. J.* **2020**, *59*, 2269–2281. [[CrossRef](#)]
- Abdeljawad, T.; Riaz, M.B.; Saeed, S.T.; Iftikhar, N.I. MHD Maxwell fluid with heat transfer analysis under ramp velocity and ramp temperature subject to non-integer differentiable operators. *Comput. Model. Eng. Sci.* **2021**, *126*, 821–841. [[CrossRef](#)]
- Firdous, H.; Saeed, S.T.; Ahmad, H.; Askar, S. Using non-Fourier's heat flux and non-Fick's mass flux theory in the radiative and chemically reactive flow of Powell-Eyring fluid. *Energies* **2021**, *14*, 6882. [[CrossRef](#)]
- Riaz, M.B.; Siddique, I.; Saeed, S.T.; Atangana, A. MHD Oldroyd-B fluid with slip condition in view of local and nonlocal kernels. *J. Appl. Comput. Mech.* **2021**, *7*, 116–127.
- Riaz, M.B.; Saeed, S.T. Comprehensive analysis of integer order, Caputo-Fabrizio and Atangana-Baleanu fractional time derivative for MHD Oldroyd-B fluid with slip effect and time dependent boundary conditions. *Discr. Contin. Dynam. Syst.* **2021**, *14*, 3719–3746. [[CrossRef](#)]
- Hazra, S.; Class, H.; Helmig, R.; Schulz, V. Forward and inverse problems in modeling of multiphase flow and transport through porous media. *Computat. Geosci.* **2004**, *8*, 21–47. [[CrossRef](#)]
- Wang, J.; Zabarar, N. A Markov random field model of contamination source identification in porous media flow. *Int. J. Heat Mass Transf.* **2006**, *49*, 939–950. [[CrossRef](#)]
- Nilssen, T.K.; Karlsen, K.H.; Mannseth, T.; Tai, X.C. Identification of diffusion parameters in a nonlinear convection-diffusion equation using the augmented lagrangian method. *Comput. Geosci.* **2009**, *13*, 317–329. [[CrossRef](#)]
- Yan, B.; Harp, D.R.; Chen, B.; Pawar, R. A physics-constrained deep learning model for simulating multiphase flow in 3D heterogeneous porous media. *Fuel* **2022**, *313*, 122693. [[CrossRef](#)]
- Yan, B.; Chen, B.; Harp, D.R.; Jia, W.; Pawar, R.J. A robust deep learning workflow to predict multiphase flow behavior during geological CO₂ sequestration injection and Post-Injection periods. *J. Hydrol.* **2022**, *607*, 127542. [[CrossRef](#)]

19. Magzymov, D.; Ratnakar, R.R.; Dindoruk, B.; Johns, R.T. Evaluation of machine learning methodologies using simple physics based conceptual models for flow in porous media. In Proceedings of the SPE Annual Technical Conference and Exhibition, Dubai, United Arab Emirates, 21–23 September 2021.
20. Almajid, M.M.; Abu-Al-Saud, M.O. Prediction of porous media fluid flow using physics informed neural networks. *J. Petrol. Sci. Eng.* **2022**, *208*, 109205. [[CrossRef](#)]
21. Jackson, D.D. Interpretation of inaccurate, insufficient and inconsistent data. *Geophys. J. R. Astron. Soc.* **1972**, *28*, 97–109. [[CrossRef](#)]
22. Watson, L.T. Globally convergent homotopy methods: A tutorial. *Appl. Math. Comput.* **1989**, *31*, 369–396.
23. Mousa, M.M.; Alsharari, F. Convergence and error estimation of a new formulation of homotopy perturbation method for classes of nonlinear integral/integro-differential equations. *Mathematics* **2021**, *9*, 2244. [[CrossRef](#)]
24. Agarwal, P.; Akbar, M.; Nawaz, R.; Jleli, M. Solutions of system of Volterra integro-differential equations using optimal homotopy asymptotic method. *Math. Meth. Appl. Sci.* **2021**, *44*, 2671–2681. [[CrossRef](#)]
25. Mousa, M.M.; Kaltayev, A. Homotopy perturbation method for solving nonlinear differential-difference equations. *Z. Naturforsch. A* **2010**, *65*, 511–517. [[CrossRef](#)]
26. Hammad, H.A.; Agarwal, P.; Guirao, J.L.G. Applications to boundary value problems and homotopy theory via tripled fixed point techniques in partially metric spaces. *Mathematics* **2021**, *9*, 2012. [[CrossRef](#)]
27. Mousa, M.M.; Kaltayev, A. Application of the homotopy perturbation method to a magneto-elastico-viscous fluid along a semi-infinite plate. *Int. J. Nonlinear Sci. Numer. Simul.* **2009**, *10*, 1113–1120. [[CrossRef](#)]
28. Saad, K.M.; Iyiola, O.S.; Agarwal, P. An effective homotopy analysis method to solve the cubic isothermal auto-catalytic chemical system. *AIMS Math.* **2018**, *3*, 183–194. [[CrossRef](#)]
29. Mallick, A.; Ranjan, R.; Das, R. Application of homotopy perturbation method and inverse prediction of thermal parameters for an annular fin subjected to thermal load. *J. Therm. Stress.* **2016**, *39*, 298–313. [[CrossRef](#)]
30. Mallick, A.; Ranjan, R.; Prasad, D.K.; Das, R. Inverse prediction and application of homotopy perturbation method for efficient design of an annular fin with variable thermal conductivity and heat generation. *Math. Model. Anal.* **2016**, *21*, 699–717. [[CrossRef](#)]
31. Biswal, U.; Chakraverty, S.; Ojha, B.K. Application of homotopy perturbation method in inverse analysis of Jeffery-Hamel flow problem. *Eur. J. Mech. B Fluid.* **2021**, *86*, 107–112. [[CrossRef](#)]
32. Sattari Shajari, P.; Shidfar, A. Application of weighted homotopy analysis method to solve an inverse source problem for wave equation. *Inverse Probl. Sci. Eng.* **2019**, *27*, 61–88. [[CrossRef](#)]
33. Liu, T. A multigrid-homotopy method for nonlinear inverse problems. *Comput. Math. Appl.* **2020**, *79*, 1706–1717. [[CrossRef](#)]
34. Liu, T. A wavelet multiscale-homotopy method for the parameter identification problem of partial differential equations. *Comput. Math. Appl.* **2016**, *71*, 1519–1523. [[CrossRef](#)]
35. Hu, L.; Huang, L.; Lu, Z.R. Crack identification of beam structures using homotopy continuation algorithm. *Inverse Probl. Sci. Eng.* **2017**, *25*, 169–187. [[CrossRef](#)]
36. Courbot, J.B.; Colicchio, B. A fast homotopy algorithm for gridless sparse recovery. *Inverse Probl.* **2021**, *37*, 025002. [[CrossRef](#)]
37. Słota, D.; Chmielowska, A.; Brociek, R.; Szczygieł, M. Application of the homotopy method for fractional inverse Stefan problem. *Energies* **2020**, *13*, 5474. [[CrossRef](#)]
38. Liu, J.; Wang, B. Solving the backward heat conduction problem by homotopy analysis method. *Appl. Numer. Math.* **2018**, *128*, 84–97. [[CrossRef](#)]
39. Liu, T. Porosity reconstruction based on Biot elastic model of porous media by homotopy perturbation method. *Chaos Soliton. Fract.* **2022**, *158*, 112007. [[CrossRef](#)]
40. Enting, I.G.; Pearman, G.I. Description of a one-dimensional carbon cycle model calibrated using techniques of constrained inversion. *Tellus B* **1987**, *39*, 459–476. [[CrossRef](#)]
41. Lambert, M.; Lesselier, D. Binary-constrained inversion of a buried cylindrical obstacle from complete and phaseless magnetic fields. *Inverse Probl.* **2000**, *16*, 563–576. [[CrossRef](#)]
42. Atzberger, C.; Richter, K. Spatially constrained inversion of radiative transfer models for improved LAI mapping from future Sentinel-2 imagery. *Remote Sens. Environ.* **2012**, *120*, 208–218. [[CrossRef](#)]
43. Auken, E.; Christiansen, A.V. Layered and laterally constrained 2D inversion of resistivity data. *Geophysics* **2004**, *69*, 752–761. [[CrossRef](#)]
44. Zhao, J.; Liu, T.; Liu, S. An adaptive homotopy method for permeability estimation of a nonlinear diffusion equation. *Inverse Probl. Sci. Eng.* **2013**, *21*, 585–604. [[CrossRef](#)]
45. Liu, T. Parameter estimation with the multigrid-homotopy method for a nonlinear diffusion equation. *J. Comput. Appl. Math.* **2022**, *413*, 114393. [[CrossRef](#)]
46. Engquist, B.; Osher, S. One-sided difference approximations for nonlinear conservation laws. *Math. Comp.* **1981**, *36*, 321–351. [[CrossRef](#)]